

Automated detector simulations and reconstruction parameterization using machine learning

D. Benjamin,¹ S. Chekanov,¹ W. Hopkins,¹ Y. Li,² and J. R. Love¹

¹*High Energy Physics Division, Argonne National Laboratory,
9700 S. Cass Avenue, Argonne, IL 60439, USA*

²*Computational Science Division, Argonne National Laboratory,
9700 S. Cass Avenue, Argonne, IL 60439, USA*

(Dated: January 27, 2020)

Abstract

Rapidly applying the effects of detector resolutions and experimental reconstruction algorithms to physics objects (e.g. electrons, muons, showers of particles) is essential in high energy physics. Currently available tools for the transformation from truth-level physics objects to reconstructed detector-level physics objects involve manually defining resolution functions. These resolution function are typically derived in bins of variables that are correlated with the resolution (e.g. pseudorapidity and transverse momentum). This process is time consuming, requires manual updates when detector conditions change, and can miss important correlations. Machine learning offers a way to automate the process of building these truth-to-reconstructed object transformation functions and can capture complex correlation of these functions for any given set of input variables. Such machine learning algorithms, with sufficient optimization, could have a wide range of applications: improving phenomenological studies by using a better detector representation, speeding up fast simulations based on parametric description of LHC detector responses, and allowing for more efficient production of Geant4 simulation by only simulating events within an interesting part of phase space.

9 I. INTRODUCTION

10 A cornerstone of particle collision experiments is Monte Carlo (MC) simulations of physics
11 processes (“truth”) followed by simulations of detector responses and object reconstruction
12 (“reco”). With increased complexity of such experiments, such as those at the Large Hadron
13 Collider (LHC), the detector simulations become increasingly complex and time consuming.
14 Parameterized detector simulations, such as Delphes [1], have been proven to be a vital
15 tool for physics performance and phenomenological studies (i.e. to estimate the sensitivity
16 of an experiment to a new physics model). An approximation of the detector responses
17 and experimental object reconstruction can, however, also be performed by neural networks
18 (NN) trained using the Geant4-based simulations that have gone through an experiment’s
19 reconstruction algorithm. This NN could then computationally rapidly transform truth MC
20 objects (jets and other identified particles) to objects modified by a detector and experi-
21 mental reconstruction algorithms.

22 The main advantage of detector parameterization based on machine learning (ML) is
23 that a neural network can automatically learn the features introduced by detailed full sim-
24 ulations, therefore, handcrafting parameters to represent resolutions and inefficiencies, as it
25 was done in Delphes and for upgrade studies, is not required. An NN trained using realistic
26 detector simulation could memorize the transformation from truth to the reco quantities
27 without manual binning of quantities by analyzers. Another advantage is that the NN ap-
28 proach can introduce a complex interdependence of variables which is currently difficult to
29 implement in parameterized simulations. Finally, since the underlying libraries used for ML
30 (e.g. Keras, pyTorch, etc) are optimized for a wide range of hardware, an NN-based truth-
31 to-reco transformation would be able to run efficiently on heterogeneous hardware resources
32 (resources that use a varied set of processors such as GPUs and CPUs).

33 As a first step towards parameterized detector simulations with ML, it is instructive to
34 investigate how a transformation from the truth to reco objects can be performed, leaving
35 aside the question of introducing objects that are created by misreconstructions or objects
36 that are lost due to inefficiencies.

II. TRADITIONAL PARAMETERIZED FAST SIMULATIONS

In abstract terms, a typical variable ξ_i^{reco} that characterizes a particle/jet, such as transverse momentum (p_T) or pseudorapidity (η), can be viewed as a multivariate transform, F , of the original variable ξ_1^{truth} at truth-level:

$$\xi_1^{\text{reco}} = F(\xi_1^{\text{truth}}, \xi_2^{\text{truth}}, \xi_3^{\text{truth}}, \dots, \xi_N^{\text{truth}}).$$

Generally, such a transform depends on several other variables $\xi_2^{\text{truth}} \dots \xi_N^{\text{truth}}$ characterizing this (or other) objects at the truth level. For example, the extent at which jet transverse momentum, p_T is modified by a detector depends on the original truth-level transverse momentum ($\xi_1^{\text{truth}} = p_T^{\text{truth}}$), pseudorapidity ($\xi_1^{\text{truth}} = \eta^{\text{truth}}$), flavor of jets and other effects that can be inferred from truth quantities. Similarly, if particular detector modules in the azimuthal angle (ϕ) are not active, this would introduce an additional dependence of this transform on ϕ .

Typical parameterized simulations ignore the full range of correlations between the variables. In most cases, the above transform is reduced to a single variable, or two (as in the case of Delphes simulations where the energy resolution of clusters depends on the original energies of particles and their positions in η). In order to take into account correlations between multiple parameters characterizing transformations to reconstruction objects a grid in the hypercube with the dimension N_b^N , where N_b is the number of histogram bins for the distributions $(\xi^{\text{reco}} - \xi^{\text{truth}})/\xi^{\text{truth}}$ representing “resolution” must be created. This methodology results in a large number of histograms when there are many correlated variables that affect the resolution.

It should be pointed out that the calculation speed for parameterized simulations of one variable that depends on N other variables at the truth level depends as N_b^N since each object at the truth level should be placed inside the grid defined by N_b bins. Therefore, complex parameterisations of resolutions and efficiencies for $N > 2$ becomes CPU intensive.

III. JET TRUTH-TO-RECO TRANSFORMATION WITH ML

To test the viability of using ML to transform truth objects to reco objects, we studied the truth-to-reco transformation for jets. Jet truth-level quantities, such as jet η , p_T , ϕ

64 and jet mass (m) are used as training inputs to an NN while the output is an array of
 65 nodes that represent the binned probability density function (PDF) of the resolution for a
 66 single variable (such as jet p_T). Additional input variables could be any variable that can
 67 influence the resolution of a jet, such as jet flavor at the truth level, jet radius, etc. Figure 1
 68 shows a schematic representation of the NN architecture for modelling detector response for
 69 a single output variable. The aim is to have the NN learn the shape of the resolution PDF,
 70 for example for the p_T , depending on other input variables such as the η of the object. A
 71 binned output (multi-categorization) was used to so that the precision of resolution PDF
 72 modelling can be selected.

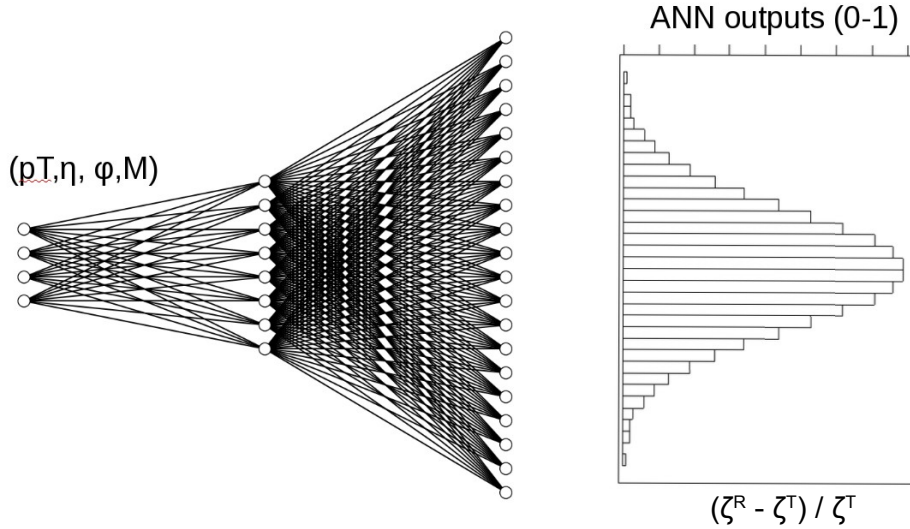


FIG. 1. A schematic representation of the NN architecture for modelling the detector response and
 affect of reconstruction algorithms on truth-level input variables. The output of this NN is a PDF
 for the resolution of single variable, e.g. $(p_T^{\text{reco}} - p_T^{\text{truth}}) / p_T^{\text{truth}}$.

73 IV. MONTE CARLO SIMULATED EVENT SAMPLES

74 Monte Carlo events used for this analysis were produced using the Madgraph generator [2].
 75 The simulated processes are a combination of equal parts top pair production ($t\bar{t}$ +jets)
 76 and photons produced in association with jets (γ +jets), which give a high rate of jets
 77 in different environments. Hadronic jets were reconstructed with the FASTJET package [3]
 78 using the anti- k_t algorithm [4] with a distance parameter of 0.4. The detector simulation was

79 performed with the Delphes package with a detector geometry which is similar to the ATLAS
 80 geometry. The event samples used in this paper, before and after the fast simulation, are
 81 available from the HepSim database [5]. In this paper only the transformation from truth
 82 jets (which have truth particle constituents) to reconstructed jets (which calorimeter cell
 83 constituent) and only for p_T was performed, however the methodology should be object and
 84 parameter agnostic. Truth jets which were matched to a reconstructed Delphes jet are used.
 85 For the matching criteria the reconstructed jet that has the smallest $\Delta R = \sqrt{\Delta\phi^2 + \Delta\eta^2}$,
 86 where $\Delta\phi = \phi^{\text{truth}} - \phi^{\text{reco}}$ and $\Delta\eta = \eta^{\text{truth}} - \eta^{\text{reco}}$, with respect to the truth jet is chosen.
 87 If this minimum ΔR is greater than 0.2, the truth jet is discarded. No other requirements
 88 are made on truth and reconstructed Delphes jets other than the $p_T > 15$ GeV requirement
 89 made by Delphes. Only matched jets are used for this study since the aim of the study is to
 90 test whether an NN can changes in detector resolution as a function of kinematic properties
 91 of the jet (e.g. p_T , η , ϕ , m). The final number of training jets used is two million while
 92 500,000 jets were used as a testing sample. The distributions of quantities used as the input
 93 for the NN, p_T , η , ϕ , m , are shown in Figure 2.

94 To facilitate gradient descent in all direction of the input variables, the input variables are
 95 scaled to be in the range [0,1]. This avoids the p_T and the mass from having a disproportional
 96 affect on the training of the NNs. The output variable, $(p_T^{\text{reco}} - p_T^{\text{truth}})/p_T^{\text{truth}}$, is also scaled
 97 to have values between 0 and 1. Only objects that are within the 1st and 99th percentile of
 98 the $(p_T^{\text{reco}} - p_T^{\text{truth}})/p_T^{\text{truth}}$ distribution are considered in this study since objects outside this
 99 range are typically not used in physics analyses.

100 V. NEURAL NETWORK STRUCTURES

101 An NN is trained with four input parameters, the scaled p_T , η , ϕ , and m , and consist
 102 of five layers with 100 nodes each and with each node having a rectifier linear unit (ReLU)
 103 activation function. The output layer has 400 nodes with a softmax activation function.
 104 Finally, the NN is trained over 1000 epochs with batch size 1000 using the Adam [6] optimizer
 105 with a learning rate of 10^{-4} . The NN is implemented using Keras [7] with a TensorFlow [8]
 106 backend.

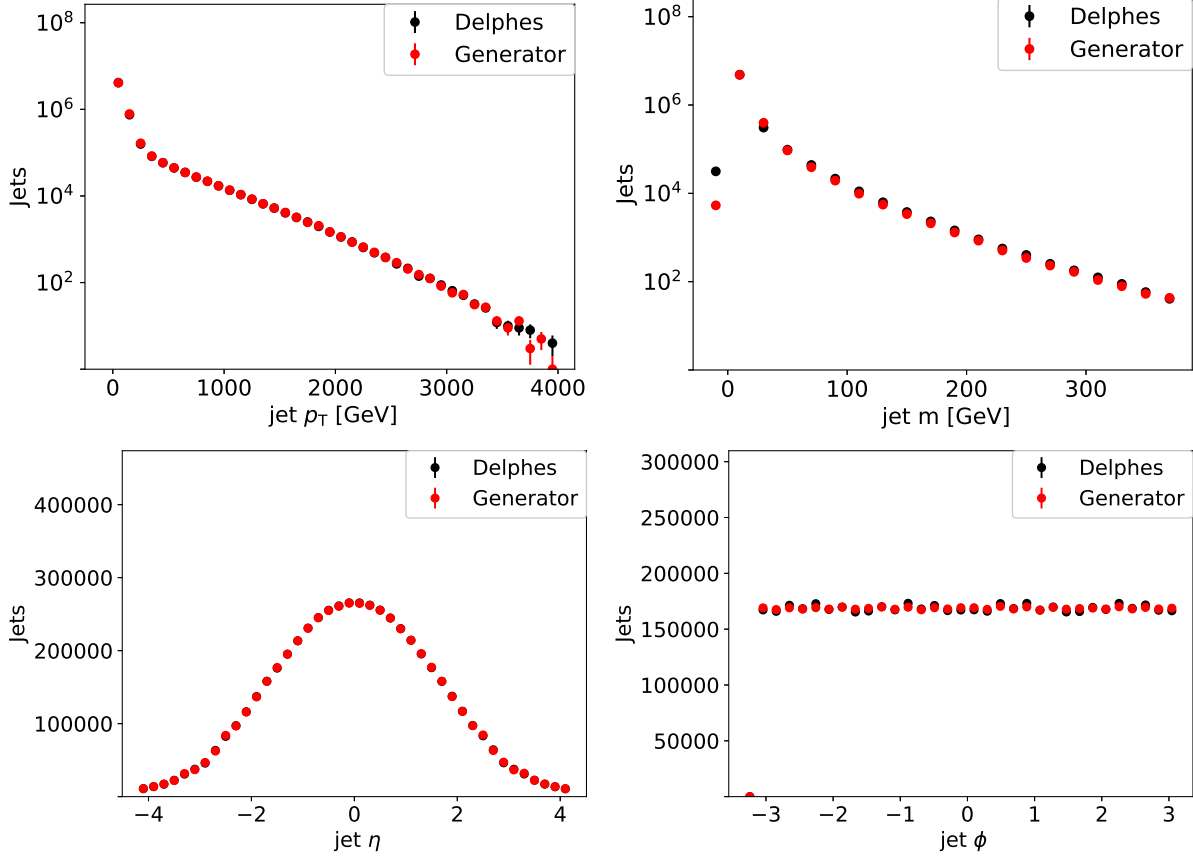


FIG. 2. Distributions for input variables for truth (red) and reco quantities (black).

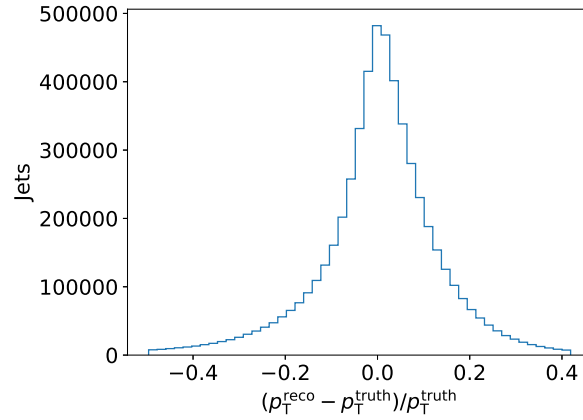


FIG. 3. Relative differences between truth and reco p_T .

107 VI. RESULTS

108 After the NN has been trained to learn the PDF of $(p_T^{\text{reco}} - p_T^{\text{truth}})/p_T^{\text{truth}}$, the resulting
 109 learned PDF is compared to the Delphes PDF using the testing sample in Fig. 4a. Good

110 agreement is observed between the Delphes and NN PDFs, showing that the NN has learned
 111 the bulk distribution.

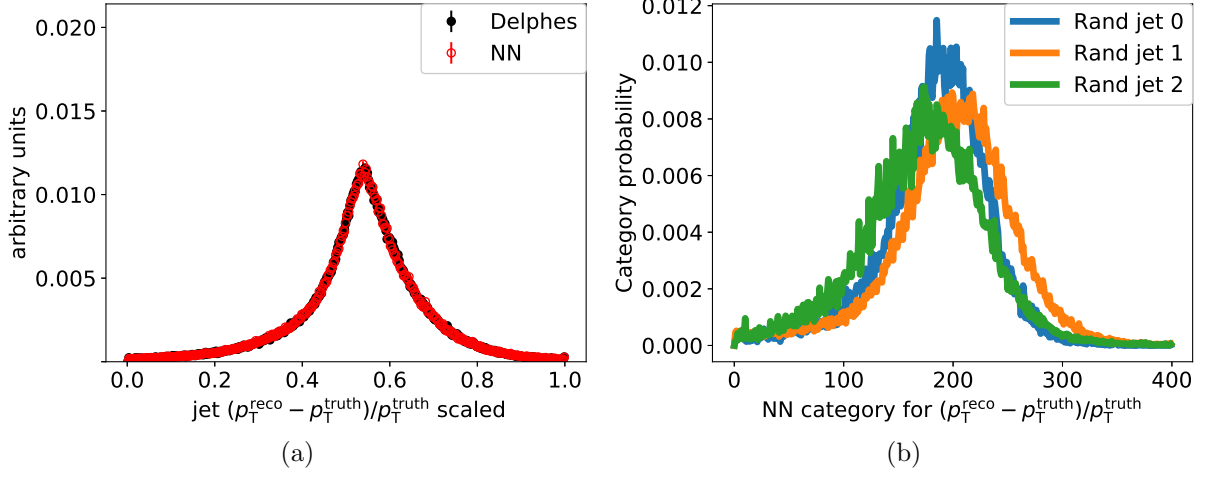


FIG. 4. NN-generated jet $(p_T^{\text{reco}} - p_T^{\text{truth}})/p_T^{\text{truth}}$ compared to reco Delphes jet $(p_T^{\text{reco}} - p_T^{\text{truth}})/p_T^{\text{truth}}$ (a). NN-generated jet PDFs for three randomly selected truth jets (b).

112 The NN predicts a PDF for each jet based on its input parameters (i.e. p_T , ϕ , η , and
 113 m). The PDFs for a set of randomly selected jets are shown in Fig. 4b. These PDFs are
 114 then randomly sampled to produce an NN jet that mimics the reco jet. A comparison of
 115 the NN-generated and Delphes jet p_T distribution for the testing sample is shown in Fig. 5.
 116 The NN reproduces the jet p_T distribution of Delphes within 5% for reconstructed jets with
 117 $p_T > 20$ GeV.

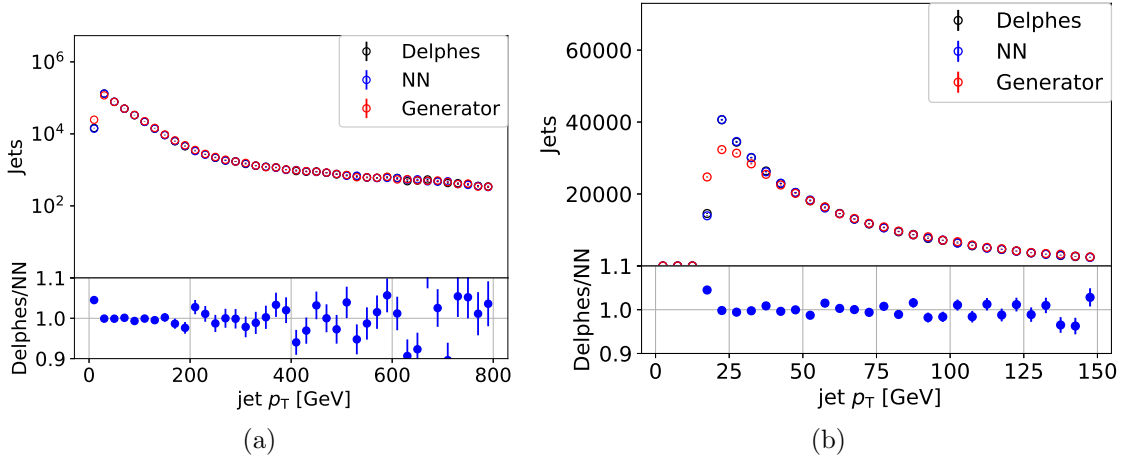


FIG. 5. Delphes and NN-generated jet p_T distributions for a wide (a) and narrow (b) p_T range.

118 To test whether the NN learned correlations between input parameters and the p_T res-

119 olution, the jets were divided into central ($|\eta| < 3.2$) and forward ($|\eta| > 3.2$) jets. The p_T
 120 resolution is then compared between the two regions for both the Delphes jets as well as the
 121 NN-generated jets. These two regions in the detector simulation have different calorime-
 122 ter resolutions which results in different jet p_T resolutions and thus the p_T resolution is
 123 correlated with $|\eta|$. The resulting resolutions for both regions are shown in Fig. 6 using
 124 the training sample. The training sample was chosen for this comparison because forward
 125 jets make up a small subsample of all jets, as can be seen in Fig. 2. Several batch-size and
 126 number-of-epoch combinations were used in an attempt to optimize the sensitivity to a small
 127 subsample (the forward jets) of the training sample. The number of backpropagations (N_{bp})
 128 were held constant by keeping the ratio of the number of epochs (N_e) and batch size (N_b)
 129 constant since $N_{bp} = \frac{N_t}{N_b} N_e$ where N_t is the number of training jets. Batch size and number
 130 of epochs of 5, 10, 20, 100, 200, 1000 were tested resulting in similar performance of the NN
 131 in both the central and forward region.

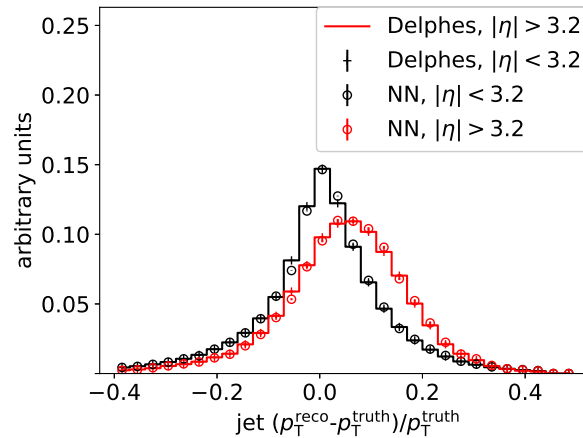


FIG. 6. Jet p_T resolution for the training sample for both the central and forward region.

132 To test whether what the NN learned is sample independent we applied the NN to a top
 133 pair production in association with a W boson ($t\bar{t}+W$) sample which contained 900,000 jets.
 134 This sample is expected to have higher jet multiplicities per event. The p_T distributions over
 135 two p_T ranges are shown in Fig. 7 while the comparison between the central and forward jet
 136 p_T resolutions can be seen in Fig. 8. The agreement in Fig. 7 is good for jets with $p_T < 200$
 137 GeV but a mismodeling trend appears at p_T s greater than 200 GeV. We expect this to be
 138 due high p_T b -jets which are not as prevalent in the training set where the high p_T jets
 139 mainly come from the γ +jets sample which is produced to have a flattened p_T spectrum.

For future studies and refinements one could add truth b -quark information to help improve the modelling of these types of jets.

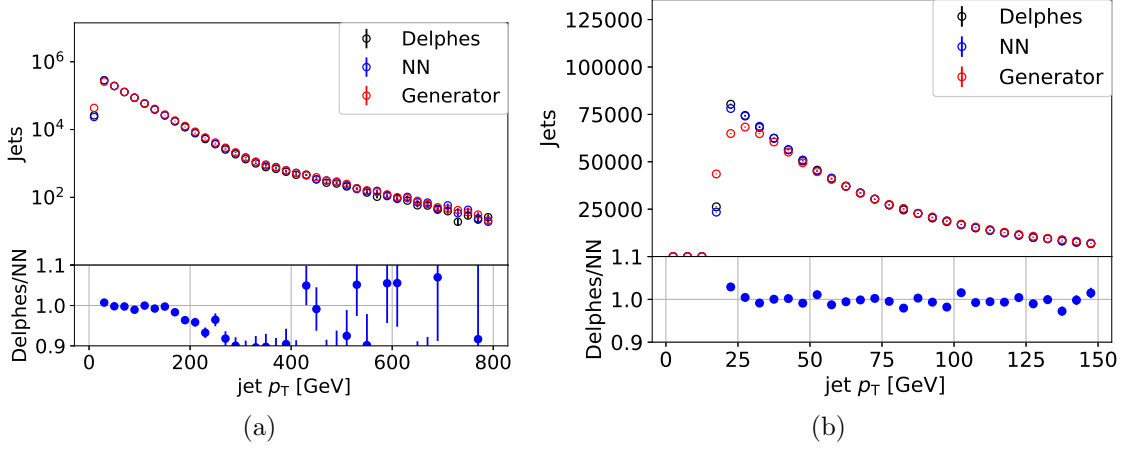


FIG. 7. Delphes and NN-generated jet p_T distributions for a wide (a) and narrow (b) p_T range for jets originating from $t\bar{t} + W$ production.

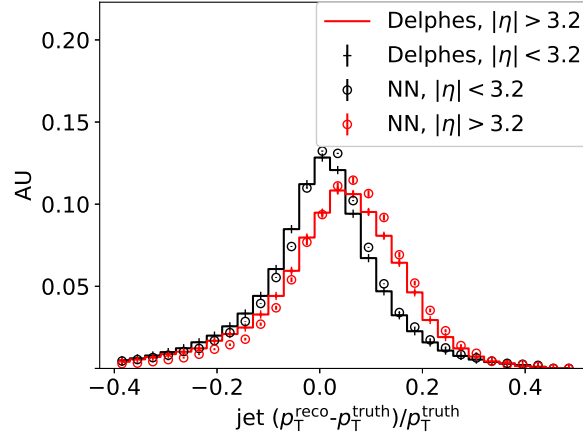


FIG. 8. Jet p_T resolution for the training sample for both the central and forward region for jets originating from $t\bar{t} + W$ production.

VII. CONCLUSION

We have shown that a truth-level quantity can be transformed to a reconstruction-level quantity using a multi-categorizing NN. The NN learned the truth-to-reconstruction transformation without requiring manual binning to capture the differences in resolutions of

particular subsamples (central and forward jets). To ensure that this method produces realistic results, the training data needs to be carefully chosen to properly represent objects that one wants to transform (as was shown in when the NN is applied to the $t\bar{t}W$). Additional improvements could be made by including more information about the objects (e.g. whether a b -quark is present in a jet, kinematic information from other objects in the event) making this method more robust. This method should be easily extendable to additional reconstructed quantities and could be used to model the ATLAS and CMS detector. The method described in this paper thus allows for automated detector parameterization which can facilitate phenomenological studies, efficient truth event selection, and upgrade studies.

ACKNOWLEDGMENTS

The submitted manuscript has been created by UChicago Argonne, LLC, Operator of Argonne National Laboratory (“Argonne”). Argonne, a U.S. Department of Energy Office of Science laboratory, is operated under Contract No. DE-AC02-06CH11357. The U.S. Government retains for itself, and others acting on its behalf, a paid-up nonexclusive, irrevocable worldwide license in said article to reproduce, prepare derivative works, distribute copies to the public, and perform publicly and display publicly, by or on behalf of the Government. The Department of Energy will provide public access to these results of federally sponsored research in accordance with the DOE Public Access Plan. <http://energy.gov/downloads/doe-public-access-plan>. Argonne National Laboratory’s work was funded by the U.S. Department of Energy, Office of High Energy Physics under contract DE-AC02-06CH11357.

-
- [1] J. de Favereau, C. Delaere, P. Demin, A. Giammanco, V. Lemaître, A. Mertens, and M. Selvaggi. DELPHES 3, A modular framework for fast simulation of a generic collider experiment. *JHEP*, 02:057, 2014.
 - [2] J. Alwall, R. Frederix, S. Frixione, V. Hirschi, F. Maltoni, et al. The automated computation of tree-level and next-to-leading order differential cross sections, and their matching to parton shower simulations. *JHEP*, 07:079, 2014.
 - [3] Matteo Cacciari, Gavin P. Salam, and Gregory Soyez. FastJet User Manual. *Eur. Phys. J. C*, 72:1896, 2012.

- 174 [4] Matteo Cacciari, Gavin P. Salam, and Gregory Soyez. The anti- k_t jet clustering algorithm.
175 *JHEP*, 04:063, 2008.
- 176 [5] S.V. Chekanov. HepSim: a repository with predictions for high-energy physics experiments.
177 *Advances in High Energy Physics*, 2015:136093, 2015. Available as <http://atlaswww.hep.>
178 [anl.gov/hepsim/](http://atlaswww.hep.anl.gov/hepsim/).
- 179 [6] Diederik P. Kingma and Jimmy Ba. Adam: A Method for Stochastic Optimization. *arXiv*
180 *e-prints*, page arXiv:1412.6980, Dec 2014.
- 181 [7] François Chollet et al. Keras. <https://keras.io>, 2015.
- 182 [8] Martín Abadi et al. TensorFlow: Large-scale machine learning on heterogeneous systems, 2015.
183 Software available from tensorflow.org.